Thermal Properties and Monolayer Films of
Cellulose Alkyl Ethers

Takahiro ITOH*, Hidematsu SUZUKI** and Takeaki MIYAMOTO***

A series of tri-O-alkyl celluloses having different n-alkyl groups were prepared, and their thermal properties and monolayer-forming behavior at the air/water interface were examined in comparison with that of the cellulose trialkanoates previously studied. The π-A isotherms of the alkyl ethers were very similar to those of the alkyl esters. However, electron microscopic observations of the transferred films revealed that the ethers formed no homogeneous film at any stage of compression, giving rise to macroscopic aggregation of molecules. The observed film thicknesses were unreasonably large. These contrast with the behavior of the esters, which formed perfectly homogeneous and stable monolayers with thickness consistent with the proposed molecular model. Since the ether derivatives are distinguished from the ester derivatives only in the linkage mode of side chain, the observed differences between them in the monolayer-forming properties are rather surprising. It is suggested that the carbonyl groups on the ester derivatives play an essential part in stabilizing the surface monolayers in terms of an energetic force or amphiphilicity (or both).

1. INTRODUCTION

Cellulose ethers are more stable to chemical conditions than other cellulose derivatives such as esters, and have been much utilized as cellulose derivatives for various functions. However, it had been difficult to prepare alkyl ether derivatives having a high degree of substitution (DS) by traditional alkali cellulose process. Recent development of non-aqueous solvent systems for cellulose[1-3] enabled us to prepare highly substituted ether derivatives such as tri-O-n-alkyl celluloses.[1]

In preceding papers[4-6], it was demonstrated that cellulose tri(n-alkanoate)s (CS) having relatively long alkyl chains form homogeneous and stable monolayer films at the air/water interface and each layer can be regularly piled up with the alkyl side chain essentially extended. Their structural homogeneity was confirmed in terms of the surface pressure (π)—area (A) isotherm and the electron microscopic observations of the fine structure

* 伊藤高廣: Tokai Senko K. K., Meieki, Nakamura-Ku, Nagoya, Aichi-Ken 464, Japan
** 鈴木秀松: Department of BioEngineering, Nagaoka University of Technology, Nagaoka, Niigata-Ken 940-21, Japan
*** 宮本武明: Institute for Chemical Research, Kyoto University, Uji, Kyoto-Fu 611, Japan

and thicknesses of the deposited films. Tri-O-n-alkyl celluloses are different from cellulose tri(n-alkanoate)s only in the linkage mode of side-chain. However, it has been recently found that cellulose tri(n-alkanoate)s having appropriate alkyl lengths form thermotropic columnar phases[7] that are remarkably different from the cholesteric phases observed for tri-O-n-alkyl celluloses.[8,9] It is essential for the molecular design of truly useful Langmuir-Blodgett films to compare the formation behavior of monolayers of tri-O-n-alkyl celluloses with that of cellulose tri(n-alkanoate)s.

In this paper, a series of tri-O-n-alkyl celluloses with varying alkyl length were prepared, and the fine structure of monolayers spread at the air/water interface was investigated by transmission electron microscopy (TEM). The results were compared with those for cellulose tri(n-alkanoate)s.

2. EXPERIMENTAL

2-1. Materials

The starting cellulose was regenerated from a commercial cellulose diacetate (Daicel Chem. Ind., viscosity-average degree of polymerization$\cong$200).[10] The completion of deacetylation was confirmed in terms of disappearance of the 1,750 cm^{-1} absorption band due to C=O stretching mode.

Dimethyl sulfoxide (DMSO) was also dried with calcium hydride and distilled under reduced pressure. Pyridine and the solvents, 1,4-dioxane and toluene, were dried with potassium hydroxide and metallic sodium, respectively. n-Alkylbromides (n-hexyl, n-decyl, n-tetradecyl and n-octadecyl bromides), purchased from Tokyo Kasei, were purified according to standard methods. The other chemicals were in guaranteed or extra pure grades.

2-2. Preparation of Tri-O-alkyl Celluloses

Four triether samples, tri-O-n-hexylcellulose (CE06), tri-O-n-decylcellulose (CE10), tri-O-n-tetradecylcellulose (CE14), and tri-O-n-octadecylcellulose (CE18) were prepared by reaction of cellulose with n-alkylbromide in the presence of NaOH.[1] The cellulose (0.65 g, 4×10^{-3} mol-equivalent) was added into 37 ml of distilled DMSO and the mixture was kept at 333 K for 30 min. After the reaction vessel was purged of air by alternatively evacuating and flushing with nitrogen, 2.6 ml of DMSO containing 30 % of SO$_2$ (0.86 g) and 1.3 ml of diethyl amine were added by syringes. During stirring at room temperature for 20 min, the cellulose was seen to be dissolved, the whole mixture becoming a transparent solution. Then, powdered NaOH (6.3 g, 1.6×10^{-1} mol) was added into the solution, which turned to be a turbid suspension. n-Alkylbromide (1.6×10^{-1} mol) was added dropwise. The reaction mixture was allowed to stand at 343 K for 20 hr, and then poured into methanol — water (10:1 by volume) mixture. The crude product was extracted with chloroform and washed with water. After the extract was redissolved in tetrahydrofuran (THF) and the insoluble impurities were removed by centrifugation, the desired ethers were precipitated with water (for CE06), methanol (for CE10 and CE14) or hot methanol (for CE18), filtered off, and washed with methanol. For further purification, the precipitation procedures were repeated several times.

2-3. Preparation of Cellulose Trialkanoates

Cellulose alkyl ester samples were prepared, using acid chloride-pyridine procedure.[10] The sample derivatives were recovered by precipitation with hot methanol for CS06, CS10, CS14 and CS18. These procedures were repeated until a sufficient purity was attained.

2-4. π-A Isotherm Measurements

Each sample was spread from its dilute solution (1×10^{-5} mol-eq in ml) in benzene (spectrograde) on a clean water surface in a Langmuir trough ($200 \times 500 \times 3$ mm^3), the temperature of which was kept at 293 K by circulating thermostated water. The subphase water was purified by using a Mitamura Riken model PLS-DFR automatic still. After 30 min was allowed for the solvent to evaporate off, the monolayer was compressed at a constant speed of 12 cm^2 min^{-1}. The surface pressure (π) was measured as a function of the area (A) by means of a film balance of a Whilhelmy type.

2-5. Observation of Monolayer Films Transferred

The surface structure of the monolayer transferred on a carbon film was observed at a direct magnification of 2,800 times by applying a dark-field imaging mode of TEM (a JEOL JEM 200-CX). By the horizontal lifting method, the monolayers were transferred, at several points of the π-A isotherm, from the water surface to a specimen copper grid (2.3 mm in diameter, 400 mesh) covered with a carbon film.[11] The film thickness was measured by a folding method; the monolayer transferred on a platinum film by the vertical lifting method was folded into two with the lining inside, and the folded edge was observed at a direct magnification of 160,000 in a bright-field imaging mode of TEM. The detail of the experimental procedure has been described before.[4,5]

2-6. Other Methods

The IR spectra were recorded with a JASCO FT IR-8000 spectrometer. ^{1}H-NMR spectra were recorded on a Varian VXR-200 spectrometer (200 MHz) in CDCl$_3$ (99.9 % purity; Aldrich) solution at room temperature.

3. RESULTS AND DISCUSSION

3-1. Sample Characterization

Figure 1 shows the IR spectra of tri-O-n-alkyl celluloses prepared, together with that of regenerated cellulose sample. Sample codes of CSn and CEn mean cellulose alkyl ester and ether derivatives having a carbon number of n in the side chain, respectively. The strong absorption bands observed for the alkyl ethers at around 2,900 and 1,450 cm^{-1} are due to the C-H stretching and bending vibrations, respectively. Complete etherification is confirmed by the almost entire disappearance of the large OH absorption at around 3,400 cm^{-1} observed for cellulose.

Table I shows the results of elemental analyses. The observed values well agree with those calculated for the corresponding alkyl celluloses with a DS value of 3.0. The DS value of samples was also checked by ^{1}H-NMR measurements. During the course of this study, however, it was found that the estimated DS values depend on the sample concentra-
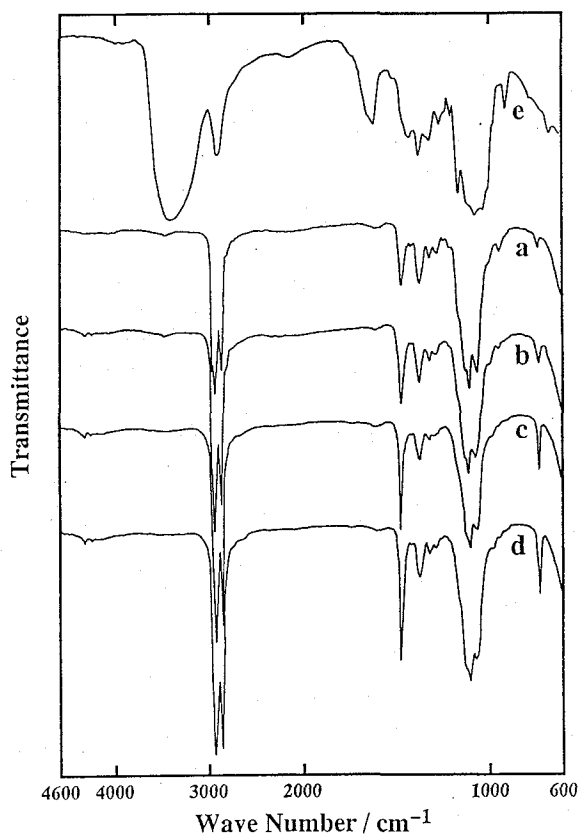
Figure 1. IR spectra of cellulose ethers; (a) CE06, (b) CE10, (c) CE14, and (d) CE18 as compared with (e) that of cellulose itself.

Table I. Elemental analyses for cellulose ethers with respect to C and H (in weight percent).

Sample	n	found		calcd	
		C	H	C	H
Tri-O-n-hexyl	6	68.99	11.21	69.52	11.18
Tri-O-n-decyl	10	73.48	12.13	74.17	12.10
Tri-O-n-tetradecyl	14	76.63	12.35	76.74	12.61
Tri-O-n-octadecyl	18	77.85	12.95	78.37	12.93

tion used for ^{1}H-NMR measurements, differing from the case of cellulose tri(n-alkanoate)s.

Figures 2a and 2b demonstrate the ^{1}H-NMR spectra of the samples CS18 and CE18 at different concentrations in CDCl$_3$, respectively. The resonance peaks of the ester derivatives are assigned as below:
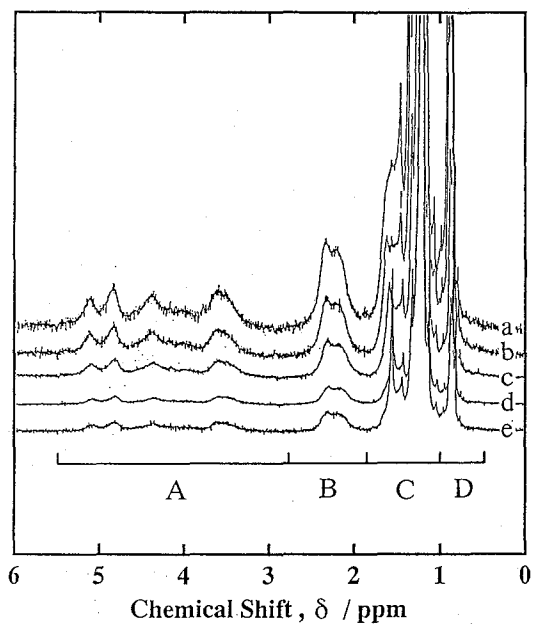
Figure 2a. ^{1}H-NMR spectra of CS18 in CDCl$_3$ solution. Each concentration is (a) 48 mmol-eq mm^{-3}, (b) 42, (c) 33, (d) 26, and (e) 19.

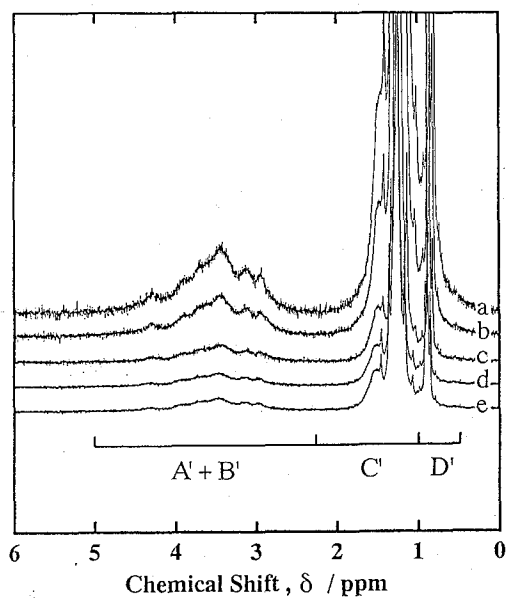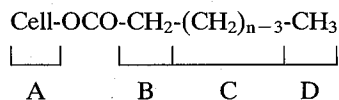Figure 2b. ^{1}H-NMR spectra of CE18 in CDCl$_3$ solution. Each concentration is (a) 37 mmol-eq mm^{-3}, (b) 31, (c) 26, (d) 20, and (e) 14.

Cell-OCO-CH$_2$-(CH$_2$)$_{n-3}$-CH$_3$

    A   B   C   D

where n represents carbon numbers of an alkyl group in the side chain. The signals of ring protons (A) of the alkyl ester derivatives are completely separated from those of methylene protons (B) adjacent to ester linkage. The DS of esterification, DS$_S$, can be easily estimated from the intensity of the methyl protons (D) by equation:

$$DS_S = 10D/(D+3A)$$

The DS value was estimated to be 3.0, independent of the polymer concentration and the side-chain length. These results indicate that the esterification of the sample is complete and the DS$_S$ value can be quantitatively estimated from the ^{1}H-NMR spectra.

On the other hand, in the case of ether derivative CE18, the signals of ring protons (A'), which appear at the lower magnetic fields, overlap with those of methylene protons (B') adjacent to ether linkages. Other alkyl protons may be assigned as shown in Figure 2.

Cell-O-CH$_2$-(CH$_2$)$_{n-2}$-CH$_3$

    A'   B'   C'   D'
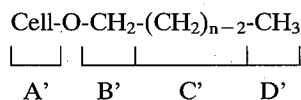
The peaks designated by C' are due to the central methylene protons in the alkyl side chains. The DS value of etherification, DS$_E$, may be estimated from the intensity of the methyl protons (D') by the equation:

$$DS_E = 10\,D'/[3(A'+B')-D']$$

where (A'+B') is the total intensity of ring protons and methylene protons adjacent to ether linkages. In Figure 3, the DS$_E$ values estimated by ^{1}H-NMR are plotted against the polymer concentration. For the derivatives with relatively long alkyl-side chains (CE18 and CE14), the DS value increases with increasing polymer concentration; i.e., the relative intensity of the ring proton signals to that of methyl proton signals decreases with increasing polymer concentration. The reason is not clear at present, but these results indicate that the molecular motion of glucose rings is more restricted than that of alkyl side chains at high polymer concentrations and the difference in the mobility increases with increasing length of the alkyl chain.

The difference in properties between ester and ether derivatives was also observed in their thermal properties. Figure 4 shows the DSC thermograms of tri-O-n-alkyl celluloses observed in a heating mode. In the ether derivatives, the samples with n≤10 exhibit only one broad peak, while the samples with n≥14 show two transitions. Photomicroscopic observations revealed that the higher-temperature peak corresponds to the anisotropic — isotropic phase transition, and the lower-temperature one, to the solid — anisotropic phase
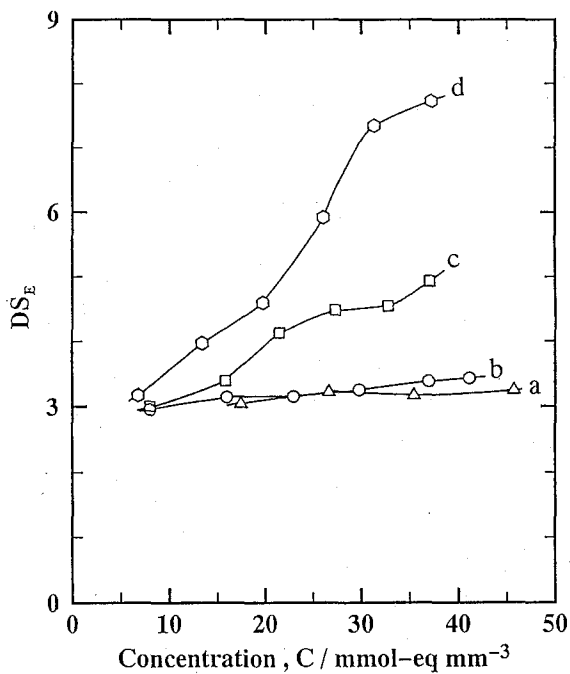
Figure 3. DS_E of (a) CE06, (b) CE10, (c) CE14, and (d) CE18 as a function of sample concentration, C.
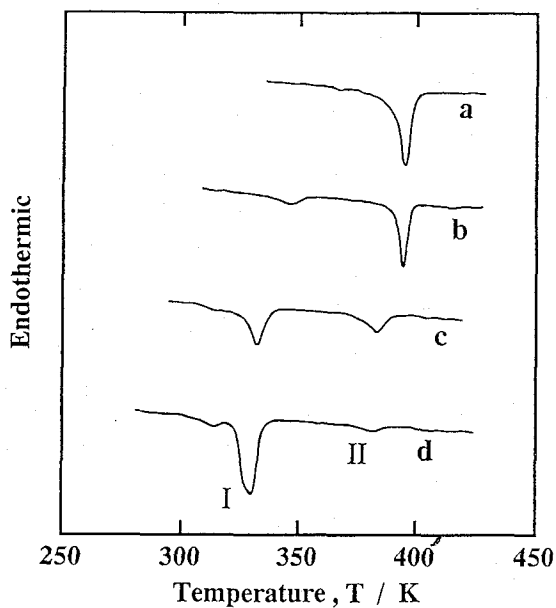

Figure 4.   DSC thermograms of cellulose tri(n-alkanoate)s; (a) CS06, (b) CS10, (c) CS14, and (d) CS18.

transition. Table II shows the phase transition temperatures estimated by photomicrosco-pic observations. These results are consistent with those already reported by Yamagishi et. al.[8,9] The cholesteric character of the mesophase was also confirmed by the microscopic observation of the striation lines attributable to the cholesteric helical repeat.

Figure 5 demonstrates the DSC thermograms of cellulose tri(n-alkanoate)s in a heating mode. Table III summarizes the phase transition temperatures of the sample derivatives. It is known that the alkyl ester derivatives having values of $n \geq 8$ cannot form cholesteric liq-uid crystalline phases but a new type of mesophases in the temperature range corresponding to peaks I and II in the DSC thermogram.[7] Recently it has been reported that the mesophase formed by these ester derivatives is of a hexagonal columnar type in which two

Table II. Phase transition temperatures of tri-O-alkyl celluloses prepared. The n is the number of carbon atoms in an alkyl side chain.

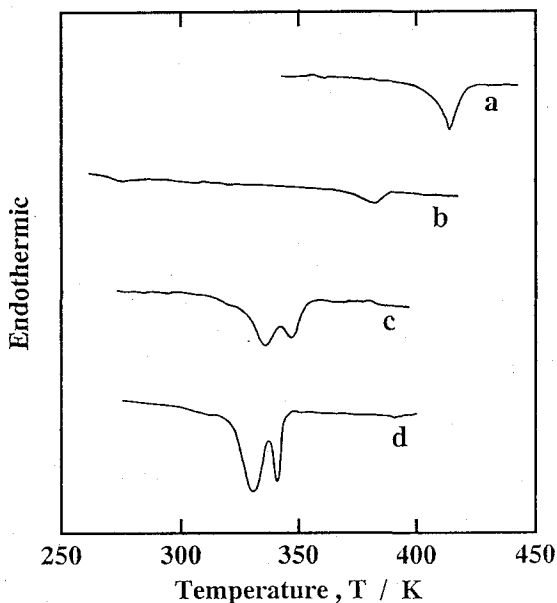| Sample	n	Phase transition temperature / K				
Tri-O-n-hexyl	6	s	370	a	410	i
Tri-O-n-decyl	10	s	290	a	370	i
Tri-O-n-tetradecyl	14	s	310	a	340	i
Tri-O-n-octadecyl	18	s	310	a	330	i

s=solid; a=anisotropic; i=isotropic

Figure 5.   DSC thermograms of tri-O-n-alkylcelluloses; (a) CE06, (b) CE10, (c) CE14, and (d) CE18.

Table III. Phase transition temperatures of cellulose tri(n-alkanoate)s. The n
is the number of carbon atoms in an alkanoyl side chain.

Sample	n	Phase transition temperature / K					
Tri(n-hexanoate)	6			s	395	i	
Tri(n-decanoate)	10	s	330	a	385	i	
Tri(n-tetradecanoate)	14	s	310	a	380	i	
Tri(n-octadecanoate)	18	s	310	a	380	i	

s=solid; a=anisotropic; i=isotropic

polymer chains are included in one hexagonal lattice.[7] To be emphasized here is that
completely different types of mesophases are formed by the difference in chemical linkage
between the main and the side chains.

3-2. π-A Isotherms

Figure 6 shows the π-A isotherms of CE10, CE14 and CE18. With increasing alkyl
length, the limiting area estimated by extrapolating the linear part of the isotherm to zero
pressure decreases, and the collapse pressure indicated by the upper end of each curve in-
creases. This may be interpreted in terms of an increase of overall cohesive force with an
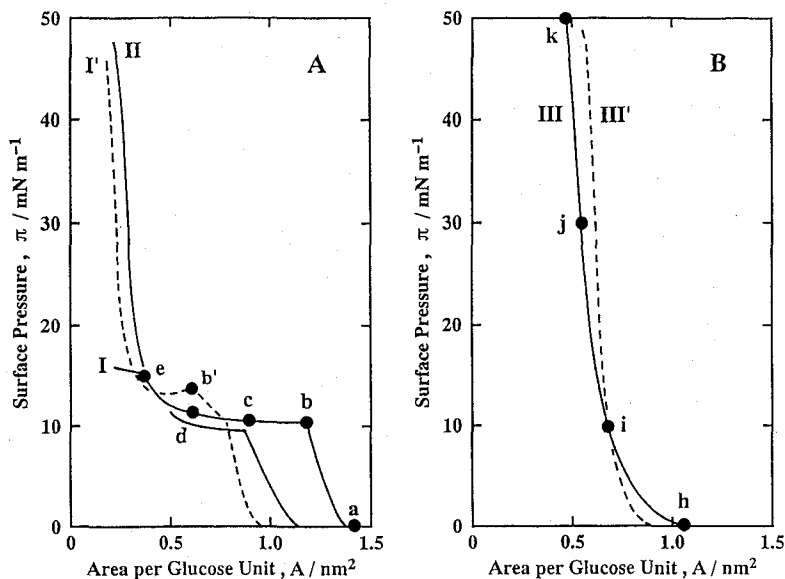increase of alkyl length. CE10 and CE14 have a plateau region in the π-A isotherm, but

Figure 6. π-A isotherms of cellulose ether derivatives at 293 K; curves I, CE10; II, CE14;
III, CE18. Points a to e and h to k denote where films were transferred. The
broken curves indicate the isotherm of the corresponding ester derivatives, CS10
(curve I') and CS18 (curve III').

CE18 does not. These results are very similar to those for the corresponding alkyl ester derivatives, CS10 and CS18, whose isotherms are shown by the broken curves in the figure (see Chapter 2). However, CE10 shows a much lower collapse pressure (15 mN m^{-1}) and a larger limiting area (1.34 nm^2) than those of CS10 (47 mN m^{-1} and 0.90 nm^2, respectively). The limiting area of CE18 is almost equal to that of CS18, but the slopes of the isotherms are different. This slope is a measure of the compressibility, hence the stability, of the surface film. The observed difference in the slope indicates that the CE18 film is less stable than the CS18 film.

3-3. Fine Structure of Monolayer Films

Figures 7a to 7e show the fine structure and thickness (inset) of the CE10 films transferred at the **a** to **e** points marked in Figure 6. In the dark-field imaging mode used for the observation of the fine structure, the objective aperture is shifted to block the main electron beam, admitting only those electrons scattered from the sample, and thus the sample film is observed as bright images on a dark background. The situation is reversed in the bright-field imaging mode. At Point **a**, where the isotherm is about to rise, the film has many holes (a few μm in size), and its thickness measures 1.3 nm. This thickness, however, should not be considered to be uniform over the whole film. At some other points of the film, it showed no measurable thickness. This means that the film is inhomogeneous, as the dark-field TEM image has shown. At Point **b**, which is the end of the first steep rise of the isotherm, the film structure is seemingly homogeneous, and the thickness measures about 1.3 nm. This thickness closely agrees with the value of 1.4 nm expected for the molecular model in which the glucose ring lies flat on the water surface with the alkyl side
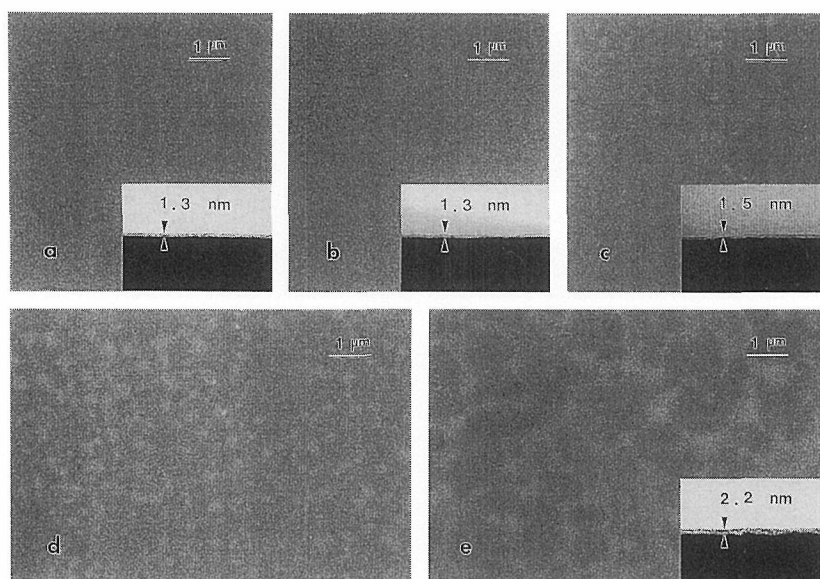

Figure 7. Dark- and bright-field images of CE10 films transferred at the corresponding points shown in Figure 6.

chains directed normal to the glucose ring.[4]   However, one should not conclude with these observations that the film at Point **b** is truly homogeneous, since the occupied area at this point (1.2 nm^2) is totally inconsistent with the value (0.59 nm^2) expected for the close-pack model.   In other words, the film density indicated by the observed thickness and occupied area is unreasonably too low.   This suggests that the film may have either many undetectable small holes or macroscopic inhomogeneities larger than the TEM sight.   This contrasts with the behavior of the ester derivative CS10, which, at the corresponding point (Point **b'**, Figure 6), gave a monolayer that fulfilled all the these criteria for a "homogeneous" film, i.e., homogeneous surface structure, reasonable film thickness, and expectable occupied area.[4]   A further compression of the CE10 film gives rise to a macroscopic aggregation of molecules (Figures 7c to 7e), eventually leading to the collapse of the film.   This collapsing pressure (15 mN m^{-1}) is much lower than that of CS10 (47 mN m^{-1}), which also indicates the instability of the ether film.

Figures 8h to 8k show the results for CE18.   No homogeneous film can be observed at any stages.   Specifically, at Point **i**, where the corresponding ester derivative CS18 formed a completely homogeneous monolayer film, this polymer gives a heterogeneous film composed of many small aggregates.   Consequently, the observed film thickness at this point (3.4 nm) is much larger than the value, 2.6 nm, expected for the n-octadecyl chains directed normal to the glucose ring, the model for CS18 (see Chapter 2).

In view of the small chemical structural difference between CE and CS, the observed differences between them in the monolayer-forming properties are rather surprising.   The carbonyl groups seem to play an essential part in stabilizing the surface monolayers in terms of an energetic interaction or amphiphilicity (or both).   It was recently found that CS forms
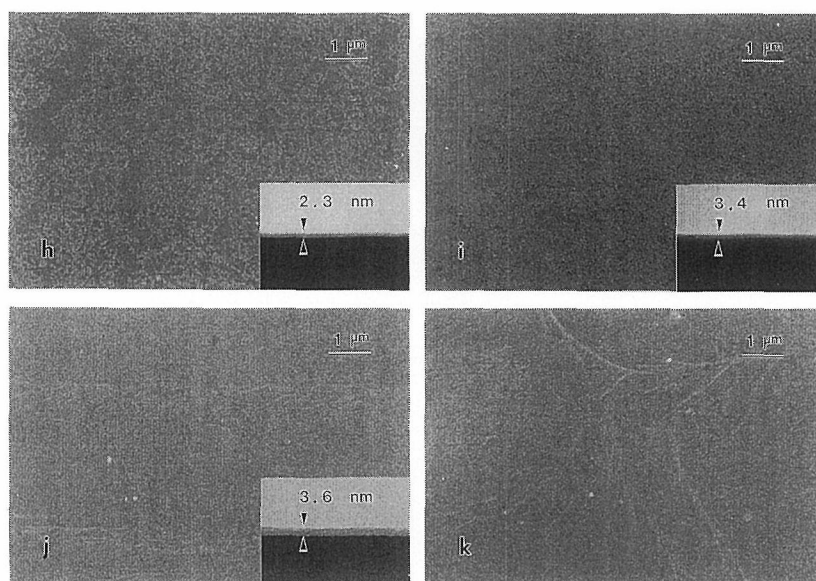

Figure 8.   Dark- and bright-field images of CE18 films transferred at the corresponding points shown in Figure 6.

a columnar liquid crystal,[7] which is a mesophase with a higher structural order than the cholesteric phase formed by CE.[8,9]   This columnar phase is believed to be stabilized by an energetic interaction in which the carbonyl groups participate.[12]

REFERENCES

1)   A. Isogai, A. Ishizu, J. Nakano, *J. Appl. Polym. Sci.*, **29,** 2097, 3873 (1984).
2)   S. M. Hudson, J. A. Cuculo, *J. Macromol. Sci., Rev. Macromol. Chem.*, **C18,** 1 (1980).
3)   C. L. McCormick, D. K. Lichatowich, *J. Polym. Sci., Polym. Lett. Ed.*, **17,** 479 (1979).
4)   T. Itoh, Y. Tujii, T. Fukuda, and T. Miyamoto, *Polym. J.*, **24,** 641 (1992).
5)   T. Itoh, Y. Tsujii, T. Fukuda, T. Miyamoto, S. Itoh, T. Asada, and M. Yamamoto, *Langmuir,* **7,** 2803 (1991).
6)   Y. Tsujii, T. Itoh, T. Fukuda, T. Miyamoto, S. Itoh, and M. Yamamoto, *Langmuir,* **8,** 936 (1992).
7)   T. Yamagishi, T. Fukuda, T. Miyamoto, Y. Yakoh, Y. Takashina, and J. Watanabe, *Liquid Cryst.,* **10,** 467 (1991).
8)   T. Yamagishi,T. Fukuda, T. Miyamoto, "Cellulose: Structural and Functional Aspects", J. F. Kennedy, G. O. Phillips, and P. A. Williams, Eds., Ellis Horwood, Chichester, 1989, p. 391.
9)   A. Takada, T. Fukuda, T. Miyamoto, and J. Watanabe, *Cell. Chem. Technol.,* **24,** 693 (1990).
10)   C. J. Malm, J. W. Mench, D. L. Kendall, G. D. Hiatt, *Ind. Eng. Chem.,* **43,** 684 (1951).
11)   R. C. Williams and R. M. Glaeser, *Science,* **175,** 1000 (1972).
12)   K. Fujii, A. Takada, T. Fukuda, and T. Miyamoto, to be published.